Journal of Nuclear Medicine, published on July 28, 2014 as doi:10.2967/jnumed.114.137562

Distinctive In Vivo Kinetics of the New Sigma$_1$ Receptor Ligands (*R*)-(+)- and (*S*)-(–)-^{18}F-Fluspidine in Porcine Brain

Peter Brust*[1], Winnie Deuther-Conrad*[1], Georg Becker[2], Marianne Patt[2], Cornelius K. Donat[1], Shannon Stittsworth[3], Steffen Fischer[1], Achim Hiller[1], Barbara Wenzel[1], Sladjana Dukic-Stefanovic[1], Swen Hesse[2], Jörg Steinbach[1], Bernhard Wünsch[4], Susan Z. Lever[3,5], and Osama Sabri[2]

[1]*Helmholtz-Zentrum Dresden-Rossendorf, Institute of Radiopharmaceutical Cancer Research, Leipzig, Germany;* [2]*Department of Nuclear Medicine and IFB Adiposity Diseases, Universität Leipzig, Leipzig, Germany;* [3]*Department of Chemistry, University of Missouri, Columbia, Missouri;* [4]*Department of Pharmaceutical and Medicinal Chemistry, Westfälische Wilhelms-Universität Münster, Münster, Germany; and* [5]*MU Research Reactor, University of Missouri, Columbia, Missouri*

Because of their involvement in growth and survival signaling cascades, the sigma$_1$ receptors (σ_1Rs) represent a novel target for the treatment of cancer and several brain diseases such as depression and neurodegeneration. From a series of σ_1R-specific ^{18}F-fluoroalkylated spirocyclic piperidines, we have chosen ^{18}F-fluspidine for detailed investigation of the in vivo kinetics of the (*R*)-(+)- and (*S*)-(–)-enantiomers to identify their potential for imaging in humans. **Methods:** Enantiopure tosylate precursors for radiolabeling were obtained using chiral preparative high-performance liquid chromatography and used for radiosynthesis of both ^{18}F-fluspidine enantiomers by nucleophilic substitution with K-^{18}F-F-Kryptofix 222-carbonate complex in a synthesis module. Brain pharmacokinetics were investigated by dynamic PET studies in piglets under baseline and blocking conditions using the highly selective σ_1R agonist SA4503. Standardized uptake values (SUVs) were calculated for 24 MR-defined brain regions. Total distribution volume (V_T) and binding potentials (k_3'/k_4) of (*S*)-(–)- and (*R*)-(+)-^{18}F-fluspidine were estimated. Furthermore, V_T values were estimated by graphical analysis using Logan plots. **Results:** The (*S*)- and (*R*)-tosylates were obtained in excellent enantiomeric purities (>98% and >96% enantiomeric excess, respectively). (*S*)-(–)- and (*R*)-(+)-^{18}F-fluspidine were synthesized within approximately 70 min (radiochemical yield, 35%–45%; specific activity, 650–870 GBq/μmol; radiochemical purity, >99%). Both radiotracers displayed different brain uptake kinetics. Although the initial brain uptake was similar, the SUV at the end of the study differed significantly ($P < 0.05$), with (*R*)-(+)-^{18}F-fluspidine showing about 60%–150% higher values. Administration of SA4503 reduced SUV almost equally for both radiotracers by approximately 65%. Furthermore, k_3' was significantly decreased under blocking conditions in almost all regions ((*S*)-(–)-^{18}F-fluspidine, −90%–95%; (*R*)-(+)-^{18}F-fluspidine, −70%–90%) whereas effects on k_4 differed according to the particular brain region. V_T estimated by both graphical analysis using Logan plots and full nonlinear kinetic analysis revealed significant inhibition for both radiotracers under blocking conditions. **Conclusion:** Both (*S*)-(–)- and (*R*)-(+)-^{18}F-fluspidine appear to be suitable for σ_1R imaging in humans. The different pharmacokinetics of (*S*)-(–)-^{18}F-fluspidine and (*R*)-(+)-^{18}F-fluspidine may have the potential for application in the diagnostics of different pathologic conditions.

Key Words: cancer; depression; sigma receptor; steroids; positron emission tomography

J Nucl Med 2014; 55:1–7
DOI: 10.2967/jnumed.114.137562

The sigma$_1$ receptor (σ_1R) is found in almost all tissues but predominantly expressed in the endocrine, immune, and nervous systems (*1*). Accordingly, there is evidence of σ_1R agonists' therapeutic potential in various neuropsychiatric diseases (supplemental data [available at http://jnm.snmjournals.org]), vascular diseases, and cancer (*2*).

Several brain-related pathologies are characterized by a decrease in the density of σ_1Rs. A reduction of 26% in postmortem ^{3}H-1, 3 di-o-tolylguanidine (DTG) binding studies was detected in the hippocampus of Alzheimer's patients (*3*), and in vivo ^{11}C-SA4503 imaging studies demonstrated a reduction of at least 25% in the regions of interest in both Parkinson's and Alzheimer's patients (*4,5*). Also, σ_1Rs might be implicated in the mechanisms of action of selective serotonin reuptake inhibitors. σ_1Rs modulate depression-related processes such as the serotonergic neurotransmission in the dorsal raphe nucleus (*6*). Antidepressants such as fluoxetine, fluvoxamine, or imipramine present high to moderate affinity for the σ_1R (affinity constant [K_i], 20–200 nM) (*7*). Repeated treatment with imipramine or fluoxetine and dl-pentazocine, a classic σ_1R ligand, caused a decrease of σ_1R density in the striatum, hippocampus, and cerebral cortex of rats (*8,9*).

The most widely investigated σ_1R ligands for PET imaging belong to piperazines or piperidines such as ^{18}F-1-(3-fluoropropyl)-4-[4-cyanophenoxy)methyl]piperidine (FPS), *N*-^{18}F-4′-fluorobenzylpiperidin-4yl-(2-fluorophenyl) acetamide, ^{18}F-fluoromethyl (FM)-SA4503, and ^{11}C-SA4503 as well as ^{18}F-labeled benzamides (references are provided in the supplemental data). ^{18}F-FPS and ^{18}F-FM-SA4503 were initially validated as suitable PET tracers; however, the uptake of ^{18}F-FM-SA4503 radiometabolites in the brain and the unfavorable brain pharmakokinetics of ^{18}F-FPS hinder evaluation of central σ_1Rs. Accumulation of radioactivity in the skull of squirrel monkeys indicates unfavorable defluorination of the novel ^{18}F-labeled benzothiazolone ^{18}F-6-(3-fluoropropyl)-3-(2-(azepan-1-yl)ethyl) benzo[d]thiazol-2(3H)-one (FTC)-146 (*10*).

Received Jan. 27, 2014; revision accepted Apr. 22, 2014.
For correspondence or reprints contact: Peter Brust, Helmholtz-Zentrum Dresden-Rossendorf, Institute of Radiopharmaceutical Cancer Research, Permoserstrasse 15, 04318 Leipzig, Germany.
E-mail: p.brust@hzdr.de
*Contributed equally to this work.
Published online ••••••••••••.

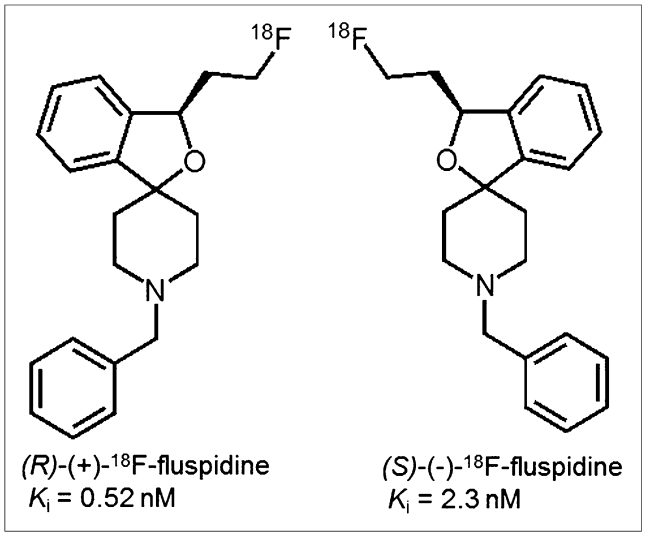

FIGURE 1. Chemical structures of the two enantiomers of ^{18}F-fluspidine.

We have recently synthesized 4 series of spirocyclic benzofurans (*11–14*) and selected 4 derivatives (K_i = 0.59–1.4 nM) for ^{18}F labeling and evaluation as PET tracers (*13–16*). Although all appear to be applicable for neuroimaging of σ_1Rs, a 2-fluoroethyl homolog, named ^{18}F-fluspidine, was most suitable (*2*). For further preclinical evaluation, an automated synthesis has been developed (*17*). Racemic fluspidine has been separated, and although the (*R*)-(+)-enantiomer (K_i = 0.57 nM) showed higher affinity than the (*S*)-enantiomer (K_i = 2.3 nM), the (*S*)-(–)-enantiomer appeared to be metabolically more stable (*18*). To test the hypothesis that both ^{18}F-fluspidine enantiomers are suitable for neuroimaging of σ_1Rs with PET, we comparatively assessed brain pharmacokinetics and specific binding of (*R*)-(+)- and (*S*)-(–)-^{18}F-fluspidine in the brain by dynamic PET studies in piglets under control and blocking conditions.

MATERIALS AND METHODS

Synthesis of Radiotracers

The radiosynthesis of (*R*)-(+)- and (*S*)-(–)-^{18}F-fluspidine (later termed [**Fig. 1**] (*R*)- and (*S*)-^{18}F-fluspidine; Fig. 1) was performed on a TRACERlab FX F-N synthesizer (GE Healthcare) according to a recently established procedure (*17*). Briefly, (*R*)- and (*S*)-^{18}F-fluspidine were radiolabeled in 15 min at 85°C starting from the corresponding enantiopure tosylate precursor obtained by separation of the racemic tosylate precursor by semipreparative chiral high-performance liquid chromatography (HPLC) on immobilized cellulose-tris-(3,5-dimethylphenyl)-carbamate as stationary phase. Radiotracers were purified by semipreparative reversed-phase HPLC and finally formulated via solid-phase extraction (specific activity, 650–870 GBq/μmol).

Confirmation of the enantiomeric purity is provided in the supplemental data.

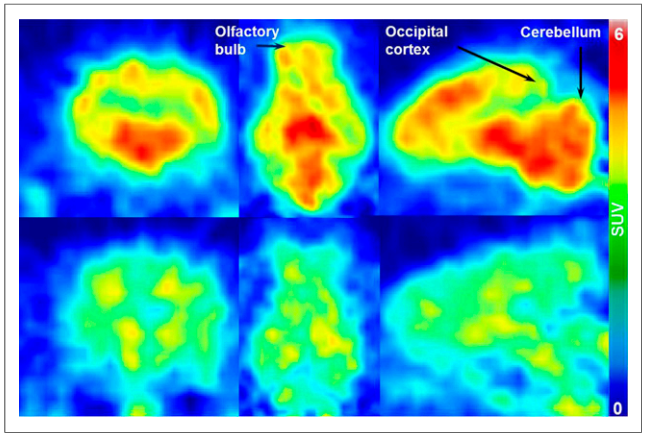

FIGURE 2. Coronal, transversal, and sagittal (left to right) PET images of two porcine brains, showing distribution of (*S*)-^{18}F-fluspidine in baseline (upper) and blocking conditions with SA4503 (lower) at 20 min after injection.

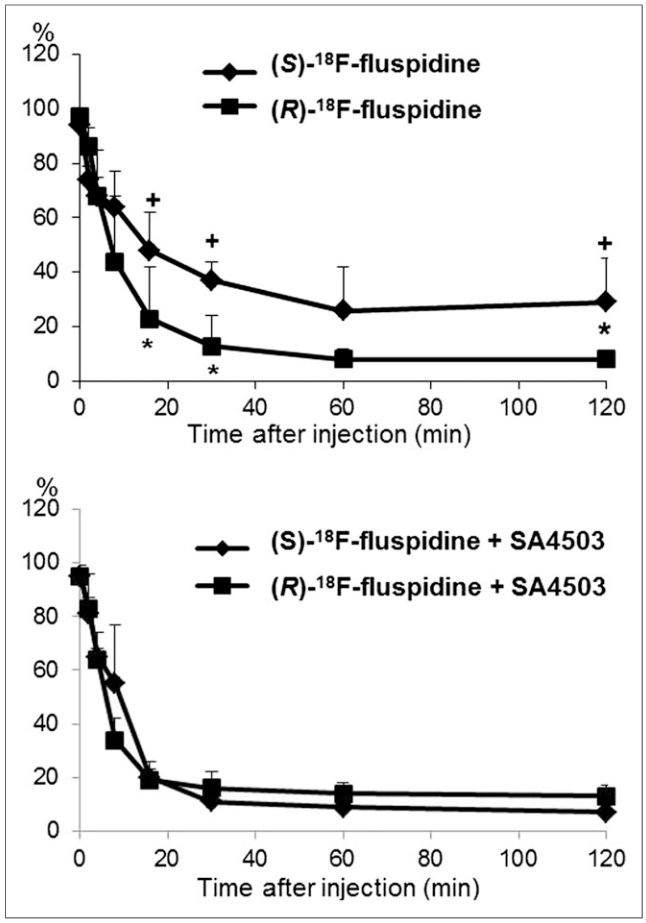

FIGURE 3. Metabolism of parent compounds. Percentage of unchanged (*S*)-^{18}F-fluspidine and (*R*)-^{18}F-fluspidine in porcine plasma dependent on time after injection under baseline (upper) and blocking conditions with SA4503 (bottom) (mean ± SD; $^*P < 0.05$ (*S*)-^{18}F-fluspidine vs. (*R*)-^{18}F-fluspidine; $^+P < 0.05$ (*S*)-^{18}F-fluspidine + SA4503 vs. (*S*)-^{18}F-fluspidine).

PET

All procedures involving animals were performed following national regulations for animal research (Landesdirektion Sachsen, TVV 22/10). Twelve female piglets (Naima × Pietrain [Agrargenossenschaft Grossdalzig], 14 ± 1 kg, 6 wk) were used. They were deprived of food but not water 24 h before delivery to the laboratory. Animals were prepared and anesthetized as described in the supplemental data.

Each radiotracer ((*R*)-^{18}F-fluspidine, 333 ± 47 MBq, n = 3; (*S*)-^{18}F-fluspidine, 353 ± 57 MBq, n = 3) was infused as a smooth bolus of 10 mL of saline into the left jugular vein over 2 min. Additional animals (n = 3 per tracer) received an administration (3 mg/kg at

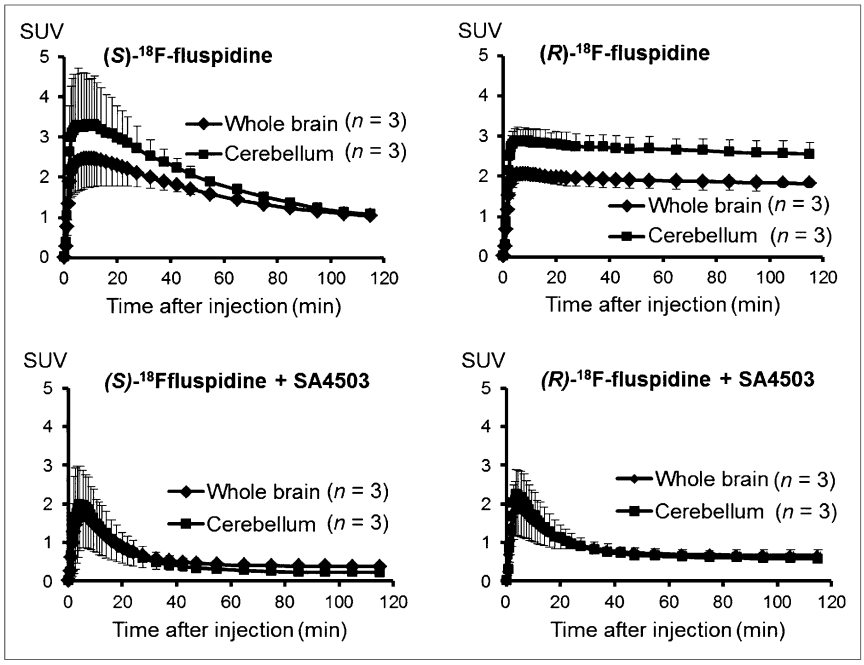

FIGURE 4. Time–radioactivity curves obtained for whole brain and cerebellum. Data represent SUVs obtained at different times after injection of (*S*)-^{18}F-fluspidine or (*R*)-^{18}F-fluspidine under baseline (upper) and blocking conditions with SA4503 (bottom) (mean ± SD).

10 min before radiotracer + 1 mg/kg/h intravenously) of the highly selective σ_1R agonist SA4503. Dynamic PET imaging (240 min; 39 frames) was performed with an ECAT EXACT HR+ (CTI/Siemens) scanner (supplemental data). Arterial blood samples (~50) were collected in intervals between 15 s and 30 min, plasma was obtained by centrifugation (15,000 rpm), and aliquots were counted in a cross-calibrated γ counter (1470 Wizard; PerkinElmer). Eight additional plasma samples were obtained for HPLC analysis of radiometabolites (details are provided in the supplemental data).

Data Analysis and Model Description

Standard procedures were used for data analysis and compartmental modeling (details are provided in the supplemental data). Because the F test and Akaike information criterion clearly revealed the preference of the 2-tissue- over the 1-tissue-compartment model, only the former data are reported. The rate constants K_1, k_2', k_3', and k_4 were estimated, and the total distribution volume (V_T) = non-displaceable distribution volume (V_{ND}) + specific distribution volume (V_S) (equal to $[K_1/k_2'][1 + k_3'/k_4]$), the V_S (equal to $[K_1/k_2'][k_3'/k_4]$), and the binding potential (BP_{ND}) ($=k_3'/k_4$) were calculated. The graphical analysis was obtained by Logan plot using metabolite-corrected plasma data with t* values fixed at 15 min for (*S*)- and 70 min for (*R*)-^{18}F-fluspidine. Data from enantiomer-specific control and blocking studies were compared and statistical significance taken as a *P* value of less than 0.05 (Student *t* test, two-tailed, unpaired).

RESULTS

Coronal, transversal, and sagittal PET images of two porcine brains acquired at 20 min after injection of (*S*)-^{18}F-fluspidine are presented in Figure 2. Activity distributions without (control; upper) and with the coadministration of SA4503 (blocking; lower) are represented in the figure. The decrease of standardized uptake values (SUVs) under blocking conditions (~50%) throughout the whole brain indicates almost ubiquitous expression of σ_1Rs. [Fig. 2]

The metabolic profiles of both radiotracers are similar, and no evidence for lipophilic radiometabolites was obtained (Supplemental Fig. 3). The metabolism of (*S*)-^{18}F-fluspidine is significantly slower than that of (*R*)-^{18}F-fluspidine (Fig. 3), which explains at least partially the significant differences in the plasma input functions (Supplemental Fig. 1). Furthermore, in contrast to (*R*)- the metabolism of (*S*)-^{18}F-fluspidine was significantly accelerated after administration of SA4503. [Fig. 3]

The time–activity curves obtained after administration of (*S*)-^{18}F-fluspidine and (*R*)-^{18}F-fluspidine reveal enantiomer-related differences in brain uptake kinetics (Fig. 4). Although the initial brain uptake is similar for both enantiomers, the SUVs at the end of the study differ significantly, with (*R*)-^{18}F-fluspidine having about 60%–150% higher values in various regions. The administration [Fig. 4]

TABLE 1
Comparison of K_1 and k_2' of (*S*)-^{18}F-Fluspidine Under Control and Blocking Conditions

	(*S*)-^{18}F-fluspidine (*n* = 3)		(*S*)-^{18}F-fluspidine + SA4503 (*n* = 3)	
Region	K_1 (mL/mL/min)	k_2' (1/min)	K_1 (mL/mL/min)	k_2' (1/min)
Frontal cortex	0.863 ± 0.127	0.235 ± 0.189	0.560 ± 0.166*	0.201 ± 0.031
Temporal cortex	0.791 ± 0.091	0.199 ± 0.135	0.469 ± 0.119*	0.174 ± 0.032
Occipital cortex	0.864 ± 0.155	0.217 ± 0.159	0.565 ± 0.156*	0.206 ± 0.057
Hippocampus	0.786 ± 0.140	0.175 ± 0.096	0.482 ± 0.185*	0.183 ± 0.036
Striatum	0.915 ± 0.150	0.213 ± 0.129	0.549 ± 0.188*	0.192 ± 0.041
Thalamus	1.152 ± 0.243	0.326 ± 0.256	0.611 ± 0.276*	0.193 ± 0.025
Colliculi	1.228 ± 0.353	0.336 ± 0.309	0.609 ± 0.254*	0.195 ± 0.034
Midbrain	1.078 ± 0.264	0.304 ± 0.211	0.477 ± 0.200*	0.184 ± 0.026
Pons	0.791 ± 0.218	0.183 ± 0.090	0.357 ± 0.157*	0.165 ± 0.017
Cerebellum	1.105 ± 0.336	0.287 ± 0.227	0.507 ± 0.143*	0.206 ± 0.054

*$P < 0.05$.

TABLE 2
Comparison of K_1 and k_2' of (*R*)-^{18}F-Fluspidine Under Control and Blocking Conditions

Region	(*R*)-^{18}F-fluspidine (n = 3)		(*R*)-^{18}F-fluspidine + SA4503 (n = 3)	
	K_1 (mL/mL/min)	k_2' (1/min)	K_1 (mL/mL/min)	k_2' (1/min)
Frontal cortex	1.053 ± 0.638	0.283 ± 0.274	0.550 ± 0.305	0.176 ± 0.031
Temporal cortex	0.969 ± 0.570	0.264 ± 0.274	0.523 ± 0.288	0.157 ± 0.027
Occipital cortex	0.981 ± 0.580	0.268 ± 0.278	0.606 ± 0.334	0.177 ± 0.046
Hippocampus	0.972 ± 0.514	0.260 ± 0.250	0.553 ± 0.277	0.177 ± 0.047
Striatum	1.147 ± 0.603	0.266 ± 0.251	0.617 ± 0.320	0.170 ± 0.043
Thalamus	1.297 ± 0.698	0.282 ± 0.263	0.683 ± 0.355	0.191 ± 0.058
Colliculi	1.427 ± 0.712	0.309 ± 0.305	0.759 ± 0.306	0.235 ± 0.079
Midbrain	1.168 ± 0.608	0.292 ± 0.288	0.651 ± 0.384	0.207 ± 0.064
Pons	0.857 ± 0.491	0.249 ± 0.252	0.475 ± 0.312	0.163 ± 0.083
Cerebellum	1.254 ± 0.681	0.315 ± 0.331	0.647 ± 0.336	0.224 ± 0.064

of SA4503 significantly reduced these SUVs, almost equally for both radioligands (~65%). This finding is confirmed by the results of the kinetic modeling.

[Table 1] [Table 2] The rates of blood–brain transfer for (*S*)- and (*R*)-^{18}F-fluspidine are shown in Tables 1 and 2. The influx rate constant K_1 and the clearance rate constant k_2' of both enantiomers do not differ significantly under control conditions. Surprisingly, the administration of SA4503 significantly reduced the K_1 of (*S*)-^{18}F-fluspidine by about 33%–56% in various regions, whereas the K_1 of (*R*)-^{18}F-fluspidine was similarly reduced but did not reach the level of [Table 3] significance because of large interindividual variability.

[Table 4] Tables 3 and 4 show the BP_{ND} values calculated for (*S*)- and (*R*)-^{18}F-fluspidine without and with the administration of SA4503. Although the mean BP_{ND} of (*S*)-^{18}F-fluspidine is about 80%–90% lower than that of (*R*)-^{18}F-fluspidine, significant differences were detected only in the frontal cortex, olfactory bulb, and colliculi. Notably, the difference in BP_{ND} of both radiotracers is mainly determined by a highly significant difference in k_4. In comparison to (*R*)-^{18}F-fluspidine, the k_4 of (*S*)-^{18}F-fluspidine is about 20-fold higher, whereas k_3' is only about 3-fold higher. SA4503 significantly decreased k_3' in almost all investigated regions ((*S*)-^{18}F-fluspidine, −90%–95%; (*R*)-^{18}F-fluspidine, −70%–90%), but the effects on k_4 depended on the particular brain region. For both enantiomers, subcortical regions were considerably less affected ((*S*)-^{18}F-fluspidine, −90%; (*R*)-^{18}F-fluspidine, −30%–60%) than cortical regions ((*S*)-^{18}F-fluspidine, −30%–60%; (*R*)-^{18}F-fluspidine, +0%–100%). Accordingly, significant decreases in BP_{ND} of both enantiomers were found only in subcortical regions such as the striatum, thalamus, colliculi, and midbrain.

Table 5 presents the whole-brain distribution volumes of the various compartments for all investigated conditions. In accordance with the previous findings, V_T of (*S*)-^{18}F-fluspidine is significantly lower than that of (*R*)-^{18}F-fluspidine, and V_T of (*R*)-^{18}F-fluspidine was significantly inhibited by SA4503. [Table 5]

Highly significant correlations were observed between the V_T values for (*S*)- and (*R*)-^{18}F-fluspidine obtained by Logan plot (Supplemental Table 1) and nonlinear analyses (Fig. 5). [Fig. 5]

DISCUSSION

The current study demonstrates the suitability of both (*S*)-^{18}F-fluspidine and (*R*)-^{18}F-fluspidine to specifically detect σ_1Rs in porcine brain by PET, thus offering two novel ^{18}F-labeled radioligands with potential to assess σ_1Rs also in humans.

This conclusion is derived from the following observations: both radioligands show a pattern characteristic for brain distribution of σ_1Rs; sufficiently high-activity uptake in the brain (SUV ~3–4), which can be blocked by the specific σ_1R ligand SA4503

TABLE 3
BP_{ND} (=k_3'/k_4) of (*S*)-^{18}F-Fluspidine Under Control and Blocking Conditions

Region	(*S*)-^{18}F-fluspidine (n = 3)			(*S*)-^{18}F-fluspidine + SA4503 (n = 3)		
	k_3' (1/min)	k_4 (1/min)	BP_{ND}	k_3' (1/min)	k_4 (1/min)	BP_{ND}
Frontal cortex	0.227 ± 0.224	0.092 ± 0.052	1.95 ± 1.35	0.011 ± 0.003	0.005 ± 0.003*	3.10 ± 2.74
Temporal cortex	0.233 ± 0.201	0.095 ± 0.048	2.05 ± 1.35	0.013 ± 0.005	0.013 ± 0.014*	2.06 ± 1.61
Occipital cortex	0.264 ± 0.223	0.113 ± 0.039	2.09 ± 1.42	0.012 ± 0.005	0.005 ± 0.003*	6.04 ± 6.41
Hippocampus	0.209 ± 0.149	0.096 ± 0.022	2.00 ± 1.35	0.017 ± 0.008*	0.031 ± 0.031*	0.87 ± 0.73
Striatum	0.250 ± 0.168	0.110 ± 0.023	2.19 ± 1.32	0.019 ± 0.015*	0.040 ± 0.043*	0.60 ± 0.33*
Thalamus	0.363 ± 0.260	0.120 ± 0.018	2.97 ± 1.89	0.009 ± 0.004*	0.041 ± 0.053*	0.57 ± 0.54*
Colliculi	0.355 ± 0.277	0.135 ± 0.024	2.66 ± 1.86	0.004 ± 0.003*	0.075 ± 0.123	1.27 ± 1.31
Midbrain	0.286 ± 0.150	0.100 ± 0.013	2.90 ± 1.51	0.013 ± 0.008*	0.071 ± 0.108	0.85 ± 0.96*
Pons	0.214 ± 0.112	0.092 ± 0.016	2.52 ± 1.71	0.019 ± 0.010*	0.024 ± 0.030*	1.76 ± 1.82
Cerebellum	0.276 ± 0.155*	0.121 ± 0.022	2.37 ± 1.30	0.014 ± 0.010*	0.036 ± 0.049*	0.89 ± 0.80

*$P < 0.05$.

jnm137562-pm ■ 7/24/14

TABLE 4
BP_{ND} ($=k_3'/k_4$) of (*R*)-^{18}F-Fluspidine Under Control and Blocking Conditions

Region	(*R*)-^{18}F-fluspidine (n = 3)			(*R*)-^{18}F-fluspidine + SA4503 (n = 3)		
	k_3' (1/min)	k_4 (1/min)	BP_{ND}	k_3' (1/min)	k_4 (1/min)	BP_{ND}
Frontal cortex	0.068 ± 0.047	0.005 ± 0.000	14.04 ± 9.23*	0.014 ± 0.008	0.002 ± 0.001†	9.57 ± 5.51
Temporal cortex	0.068 ± 0.044†	0.005 ± 0.001	15.74 ± 11.37	0.014 ± 0.006	0.003 ± 0.001†	4.74 ± 2.28
Occipital cortex	0.069 ± 0.047	0.005 ± 0.001*	15.21 ± 11.69*	0.019 ± 0.015	0.003 ± 0.001†	9.33 ± 5.29
Hippocampus	0.071 ± 0.047	0.005 ± 0.001*	16.39 ± 12.78	0.012 ± 0.004†	0.009 ± 0.005	1.65 ± 1.04
Striatum	0.070 ± 0.045	0.005 ± 0.001*	14.33 ± 10.26	0.009 ± 0.04†	0.011 ± 0.006	0.87 ± 0.30†
Thalamus	0.076 ± 0.041	0.006 ± 0.002‡	15.02 ± 10.26	0.007 ± 0.002†	0.008 ± 0.003	0.89 ± 0.35†
Colliculi	0.078 ± 0.038	0.006 ± 0.002‡	14.78 ± 9.48*	0.006 ± 0.001†	0.007 ± 0.002	0.84 ± 0.42†
Midbrain	0.080 ± 0.040	0.005 ± 0.002‡	17.23 ± 11.95	0.011 ± 0.008†	0.007 ± 0.001	1.76 ± 1.51†
Pons	0.082 ± 0.048	0.004 ± 0.002‡	26.52 ± 25.83	0.054 ± 0.059	0.009 ± 0.006	5.19 ± 2.53
Cerebellum	0.083 ± 0.050	0.006 ± 0.002‡	17.25 ± 13.42	0.015 ± 0.008†	0.005 ± 0.002	3.75 ± 2.62

*$P < 0.05$ and ‡$P < 0.01$ vs. (*S*)-^{18}F-fluspidine.
†$P < 0.05$ vs. (*R*)-^{18}F-fluspidine.

by about 65%; and SA4503-induced inhibition of the association rate constant k_3' of receptor binding by more than 70%.

Racemic ^{18}F-fluspidine shows a high selectivity for the σ_1R over the σ_2R (1,300-fold), the vesicular acetylcholine transporter (2,400-fold), the emopamil binding protein (360-fold), and further off-target proteins (>600-fold) (*16*). By contrast, nonnegligible affinity (50 nM) of SA4503 to the vesicular acetylcholine transporter has been observed (*19*). Considering the importance of cholinergic innervation in the regulation of cerebral circulation, we assume an anticholinergic effect of SA4503 on cerebral blood flow to explain the reduced blood–brain transfer (K_1) of (*S*)-^{18}F-fluspidine and (*R*)-^{18}F-fluspidine in porcine brain detected under blocking conditions.

Fast metabolism of ^{11}C-SA4503 (74% metabolized at 15 min after injection in cats) (*20*) was originally regarded as a disadvantage. The present study shows that (*R*)-^{18}F-fluspidine is metabolized in pigs to almost the same extent (~77% metabolized at 16 min after injection). However, (*S*)-^{18}F-fluspidine is significantly more stable (52% metabolized at 16 min after injection), suggesting stereospecific metabolism as previously shown for other drugs (*21*). Furthermore, metabolism in humans may differ from animals, as reflected by a considerably lower metabolism of (+)-^{18}F-FMe-McN5652 in humans in comparison to pigs (*22*).

TABLE 5
Distribution Volumes of (*S*)-^{18}F-Fluspidine and (*R*)-^{18}F-Fluspidine in Whole Brain

Compound	Distribution volumes (mL g^{-1})		
	V_{ND} ($=K_1/k_2'$)	V_S	V_T
(*S*)-^{18}F-fluspidine	6.28 ± 5.07	6.79 ± 2.48	13.07 ± 3.36
+ SA4503	2.42 ± 0.92	6.73 ± 4.46	9.14 ± 5.08
(*R*)-^{18}F-fluspidine	4.86 ± 2.51	82.6 ± 91.2	132.7 ± 53.9*
+ SA4503	2.90 ± 1.64	14.21 ± 8.41	22.62 ± 5.54†

*$P < 0.05$ vs. (*S*)-^{18}F-fluspidine.
†$P < 0.05$ vs. (*R*)-^{18}F-fluspidine.

In conformity with various kinetic models used to quantify σ_1R availability by ^{11}C-SA4503-PET (*2*), we applied full kinetic analysis for fitting a 2-tissue-compartment model to the dynamic PET data to determine BP_{ND} and V_T of (*S*)-^{18}F-fluspidine and (*R*)-^{18}F-fluspidine. The reference tissue model is not applicable because σ_1Rs are present in all brain regions (*23*).

In comparison to the values reported for ^{11}C-SA4503 in humans (*24*), (*S*)-^{18}F-fluspidine possesses lower and (*R*)-^{18}F-fluspidine higher BP_{ND} and V_T values. Regarding the two novel tracers, V_T values obtained from full kinetic and Logan plot analyses are highly correlated, indicating the applicability of both radioligands for clinical imaging, although graphical analysis points to differences in t* as start time for linearization (*25*). A shorter equilibration period of (*S*)-^{18}F-fluspidine and significantly higher k_4 values in comparison to (*R*)-^{18}F-fluspidine support the clinical applicability of (*S*)-^{18}F-fluspidine due to shorter scanning times. We would like to point out the differences in BP_{ND}, a function of the affinity constant of the PET tracer (K_D), and the receptor density (B_{max}), with 5- to 10-fold higher values of the (*R*)-enantiomer in comparison to the (*S*)-enantiomer. As B_{max} of a particular receptor has to be assumed to be independent from the receptor-specific PET tracer under investigation, this discrepancy may be related at least partially to the 4-fold-higher affinity toward σ_1R of (*R*)-fluspidine in comparison to (*S*)-fluspidine (*18*). Besides, endogenous compounds interacting with the steroid-binding component of σ_1Rs (details are provided in the supplemental data) could affect the lower-affine (*S*)-^{18}F-fluspidine more than the higher-affine (*R*)-^{18}F-fluspidine.

Highly specific binding of both tracers as demonstrated by inhibition of the PET signal with SA4503 (64% and 89% for (*S*)- and (*R*)-^{18}F-fluspidine, respectively) indicates that both (*S*)-^{18}F-fluspidine and (*R*)-^{18}F-fluspidine have potential for quantitative neuroimaging of σ_1Rs in human studies. For example, comparison of BP_{ND} for σ_1Rs by ^{11}C-SA4503 PET revealed a 55% reduction in the thalamus of patients with Alzheimer's disease in comparison to healthy controls (*4*) and a 30% reduction in the more-affected than in the less-affected side of the anterior putamen in patients with Parkinson's disease (*5*) (further details are provided in the supplemental data). Besides, (*S*)-^{18}F-fluspidine is assumed to be applicable in receptor occupancy studies investigating, for example, the binding of selected selective serotonin reuptake inhibitors toward

jnm137562-pm ■ 7/24/14

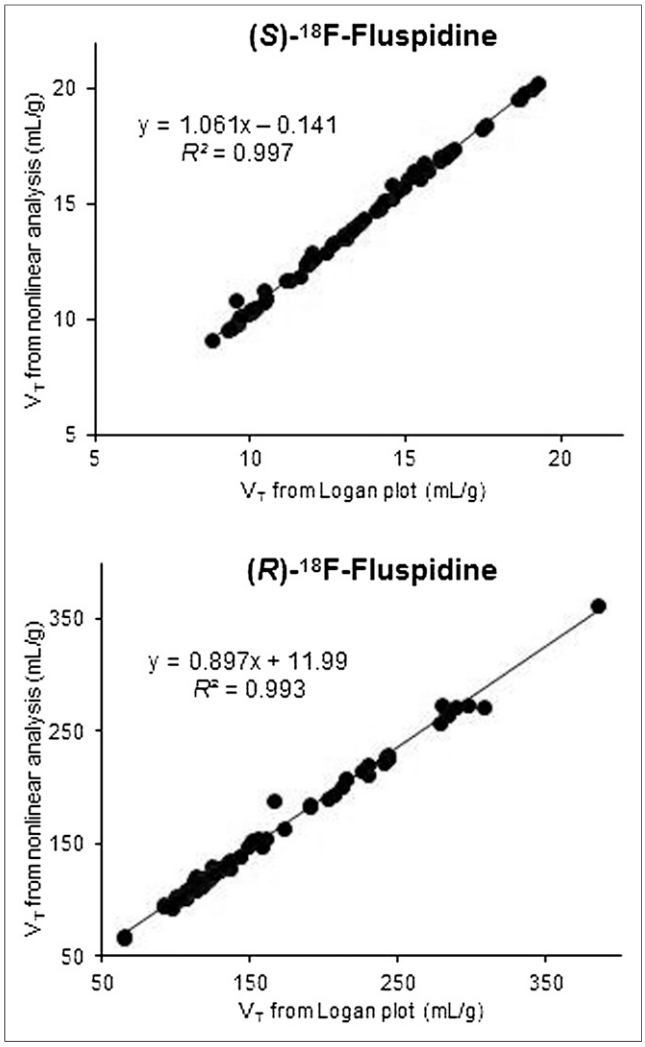

FIGURE 5. Linear correlation of values of V_T estimated for (*S*)-^{18}F-fluspidine (upper) and (*R*)-^{18}F-fluspidine (bottom) by compartment model analysis and Logan plot analysis. Values from all control subjects for all regions of interest are plotted.

σ_1Rs such as recently shown by PET studies in humans using fluvoxamine. At therapeutic doses, this drug decreased regional BP_{ND} values of ^{11}C-SA4503 by up to 35% of the control and occupied up to 60% of the available σ_1Rs. This result not only implicates an activity of fluvoxamine at σ_1Rs in the mechanisms of the action of this particular selective serotonin reuptake inhibitor (*26*) but also demonstrates the significance of PET imaging of σ_1R in humans for improved understanding of depressive disorders (*2*).

Altogether, the current preclinical data obtained by comparative PET studies using (*S*)- and (*R*)-^{18}F-fluspidine indicate the general suitability of both tracers because specific binding seems to be sufficient to assess the expected changes in receptor availability in different brain diseases. (*R*)-^{18}F-fluspidine possesses a 4-fold-higher affinity in vitro, which is translated into higher BP_{ND} values in vivo; however, longer equilibration periods require longer scanning times. The higher metabolic stability of (*S*)-^{18}F-fluspidine results in a more reliable estimate of the metabolite-corrected plasma input function required for kinetic modeling of PET tracers for central σ_1Rs due to the lack of a receptor-free reference region. For measuring σ_1R occupancy by either administered drugs or endogenous ligands, the lower-affine and thus faster dissociating (*S*)-^{18}F-fluspidine also seems to be more appropriate because of a higher susceptibility to the competitive compounds.

Although (*S*)-^{18}F-fluspidine is the more suitable enantiomer for imaging of central σ_1Rs, for the selection of one enantiomer for diagnostic imaging of peripheral changes in σ_1Rs related to pathologic processes, further data on pharmacokinetics in, for example, cancerous tissue may be required.

The concept of in vivo targeting of σ_1Rs by molecular imaging with PET has the potential for both drug development and evaluation of potential therapeutics (*27*) and pathogenesis research and clinical diagnosis.

CONCLUSION

The results of our preclinical study suggest that with (*S*)-^{18}F-fluspidine and (*R*)-^{18}F-fluspidine, two novel PET tracers for the noninvasive visualization and quantification of σ_1Rs are available. Further experimental data will be required to support the selection of the most appropriate enantiomer of ^{18}F-fluspidine for particular human translation.

DISCLOSURE

The costs of publication of this article were defrayed in part by the payment of page charges. Therefore, and solely to indicate this fact, this article is hereby marked "advertisement" in accordance with 18 USC section 1734. Financial support was obtained from German Research Council (DFG) (STE 601/10-2, WU 176/7-2) and NIH (T32 EB004822). No other potential conflict of interest relevant to this article was reported.

REFERENCES

1. Hashimoto K. Sigma-1 receptor chaperone and brain-derived neurotrophic factor: emerging links between cardiovascular disease and depression. *Prog Neurobiol.* 2013;100:15–29.
2. Brust P, Deuther-Conrad W, Lehmkuhl K, Jia H, Wünsch B. Molecular imaging of σ_1 receptors in vivo: current status and perspectives. *Curr Med Chem.* 2014;21:35–69.
3. Jansen KL, Faull RL, Storey P, Leslie RA. Loss of sigma binding sites in the CA1 area of the anterior hippocampus in Alzheimer's disease correlates with CA1 pyramidal cell loss. *Brain Res.* 1993;623:299–302.
4. Mishina M, Ohyama M, Ishii K, et al. Low density of sigma1 receptors in early Alzheimer's disease. *Ann Nucl Med.* 2008;22:151–156.
5. Mishina M, Ishiwata K, Ishii K, et al. Function of σ_1 receptors in Parkinson's disease. *Acta Neurol Scand.* 2005;112:103–107.
6. Bermack JE, Debonnel G. The role of sigma receptors in depression. *J Pharmacol Sci.* 2005;97:317–336.
7. Villard V, Meunier J, Chevallier N, Maurice T. Pharmacological interaction with the sigma1 (σ1)-receptor in the acute behavioral effects of antidepressants. *J Pharmacol Sci.* 2011;115:279–292.
8. Shirayama Y, Nishikawa T, Umino A, Takahashi K. p-chlorophenylalanine-reversible reduction of σ binding sites by chronic imipramine treatment in rat brain. *Eur J Pharmacol.* 1993;237:117–126.
9. Shirayama Y, Nishikawa T, Takahashi K. Differential effects of repeated dl-pentazocine treatment on σ binding sites in discrete brain areas of the rat. *Neurosci Lett.* 1994;165:219–222.
10. James ML, Shen B, Nielsen CH, et al. Evaluation of σ_1 receptor radioligand ^{18}F-FTC-146 in rats and squirrel monkeys using PET. *J Nucl Med.* 2014;55:147–153.
11. Grosse Maestrup E, Wiese C, Schepmann D, et al. Synthesis of spirocyclic σ_1 receptor ligands as potential PET radiotracers, structure-affinity relationships and in vitro metabolic stability. *Bioorg Med Chem.* 2009;17:3630–3641.
12. Maestrup EG, Wiese C, Schepmann D, Brust P, Wünsch B. Synthesis, pharmacological activity and structure affinity relationships of spirocyclic σ_1 receptor

ligands with a (2-fluoroethyl) residue in 3-position. *Bioorg Med Chem.* 2011; 19:393–405.
13. Maisonial A, Grosse Maestrup E, Fischer S, et al. A ^{18}F-labeled fluorobutyl-substituted spirocyclic piperidine derivative as a selective radioligand for PET imaging of σ_1 receptors. *ChemMedChem.* 2011;6:1401–1410.
14. Maisonial A, Grosse Maestrup E, Wiese C, et al. Synthesis, radiofluorination and pharmacological evaluation of a fluoromethyl spirocyclic PET tracer for central σ_1 receptors and comparison with fluoroalkyl homologs. *Bioorg Med Chem.* 2012;20:257–269.
15. Maestrup EG, Fischer S, Wiese C, et al. Evaluation of spirocyclic 3-(3-fluoropropyl)-2-benzofurans as σ_1 receptor ligands for neuroimaging with positron emission tomography. *J Med Chem.* 2009;52:6062–6072.
16. Fischer S, Wiese C, Grosse Maestrup E, et al. Molecular imaging of sigma receptors: synthesis and evaluation of the potent σ_1 selective radioligand [^{18}F] fluspidine. *Eur J Nucl Med Mol Imaging.* 2011;38:540–551.
17. Maisonial-Besset A, Funke U, Wenzel B, et al. Automation of the radiosynthesis and purification procedures for [^{18}F]fluspidine preparation, a new radiotracer for clinical investigations in PET imaging of σ_1 receptors in brain. *Appl Radiat Isot.* 2014;84:1–7.
18. Holl K, Falck E, Köhler J, et al. Synthesis, characterization and metabolism studies of fluspidine enantiomers. *ChemMedChem.* 2013;8:2047–256.
19. Ishiwata K, Kawamura K, Yajima K, QingGeLeTu, Mori H, Shiba K. Evaluation of (+)-p-[^{11}C]methylvesamicol for mapping σ_1 receptors: a comparison with [^{11}C]SA4503. *Nucl Med Biol.* 2006;33:543–548.
20. Kawamura K, Ishiwata K, Shimada Y, et al. Preclinical evaluation of [^{11}C]SA4503: radiation dosimetry, in vivo selectivity and PET imaging of σ_1 receptors in the cat brain. *Ann Nucl Med.* 2000;14:285–292.
21. Rentsch KM. The importance of stereoselective determination of drugs in the clinical laboratory. *J Biochem Biophys Methods.* 2002;54:1–9.
22. Hesse S, Brust P, Mäding P, et al. Imaging of the brain serotonin transporters (SERT) with ^{18}F-labelled fluoromethyl-McN5652 and PET in humans. *Eur J Nucl Med Mol Imaging.* 2012;39:1001–1011.
23. Sakata M, Kimura Y, Naganawa M, et al. Shortened protocol in practical [^{11}C]SA4503-PET studies for sigma$_1$ receptor quantification. *Ann Nucl Med.* 2008;22:143–146.
24. Sakata M, Kimura Y, Naganawa M, et al. Mapping of human cerebral σ_1 receptors using positron emission tomography and [^{11}C]SA4503. *Neuroimage.* 2007;35:1–8.
25. Logan J. Graphical analysis of PET data applied to reversible and irreversible tracers. *Nucl Med Biol.* 2000;27:661–670.
26. Ishikawa M, Ishiwata K, Ishii K, et al. High occupancy of σ1 receptors in the human brain after single oral administration of fluvoxamine: a positron emission tomography study using [^{11}C]SA4503. *Biol Psychiatry.* 2007;62:878–883.
27. Waterhouse RN, Chang RC, Atuehene N, Collier TL. In vitro and in vivo binding of neuroactive steroids to the σ_1 receptor as measured with the positron emission tomography radioligand [^{18}F]FPS. *Synapse.* 2007;61:540–546.